3D simulation of overtopping erosion on embankments by shallow-water approximation

Simulation en 3D d'une érosion par débordement sur des remblais, avec approximation en eau peu profonde

Fujisawa K., Murakami A.
Graduate School of Agriculture, Kyoto University, Kyoto 606-8530, Japan

ABSTRACT: Recently, the failure of embankments, such as levees and small embankment dams for irrigation reservoirs, has occurred more frequently because of a greater chance of severe typhoons and localized heavy rains. Overflow, a phenomenon in which the water level exceeds the height of the embankments, is known as a primary cause of embankment breaks. The purpose of this study is to develop a numerical method which can predict the breach process of an embankment caused by overflow. This paper presents the three-dimensional numerical analysis of embankment breaching. The finite volume method, with a Riemann solver, is applied to numerically solve shallow water equations for computing the overflow onto the embankments and the changes in configuration of the embankment profiles are successively calculated in accordance with the erosion rates of the embankment materials as a function of the bed shear stress exerted onto the embankment surface. In order to achieve a stable computation, the surface gradient method is incorporated into the finite volume discretization. The proposed method has enabled three dimensional breaching of embankments to be stablely computed.

RÉSUMÉ : Récemment, les défaillances des remblais comme les digues et les petits barrages en remblais pour les réservoirs d'irrigation, se produisent plus fréquemment en raison d'une augmentation des typhons violents et de fortes pluies localisées. Le débordement, phénomène dans lequel le niveau d'eau dépasse la hauteur des remblais, est connu comme étant la principale cause de rupture des remblais. L'objectif de cette étude est de développer une méthode numérique qui permette de prédire le processus d'une rupture de remblai causée par débordement. Cet article présente l'analyse numérique tridimensionnelle d'une rupture de remblai. La méthode des volumes finis, avec un solveur de Riemann, est appliquée pour résoudre numériquement des équations en eau peu profonde pour le calcul du trop-plein sur le remblai, et les changements dans la configuration du profil du remblai sont successivement calculés selon les taux d'érosion des matériaux de remblai en fonction de la contrainte de cisaillement exercée sur la surface du remblai. Afin de réaliser un calcul stable, la méthode du gradient de surface est incorporée dans la discrétisation par les volumes finis. La méthode proposée a permis d'effectuer des calculs très stables de ruptures de remblais en trois dimensions.

KEYWORDS: embankment, overtopping, overflow, erosion, numerical simulation, shallow water equations

1 INTRODUCTION

Recently, the failure of embankments, such as levees and small embankment dams for irrigation reservoirs, has occurred more frequently because of a greater chance of severe typhoons and localized heavy rains. Overflow, a phenomenon in which the water level exceeds the height of the embankments, is known as a primary cause of embankment breaks. Actually, Foster et al. (2000) statistically investigated the failure and the incidents involving embankment dams around the world, and reported that such failure accounted for approximately 50% of these incidents. Overflow is a major threat to embankments made of earth materials; and thus, interest in the failure of embankments triggered by overflow has been growing. Visser (1998) and Coleman et al. (2002) investigated the breaching process of cohesionless embankments during overtopping failure, while Zhu (2006) focused his investigation on the failure process of cohesive embankments. Hanson et al. (2005) conducted large-scale overflow-embankment tests using silty sand and a clayey material, and Hanson et al. (2011) integrated the material properties for embankment breach.

This paper is dedicated to develop a tool to compute the three dimensional breaching process of embankments caused by overflow, since it enables the damage to the earth structure and the time up its break to be predicted in advance of severe events, such as typhoons, floods and tsunamis. This paper presents a numerical analysis of embankment erosion using shallow water equations, which are often applied to the computation of overland flows. The finite volume approach, combined with the surface gradient technique (Zhou et al. 2001), is applied to numerically solve shallow water equations for computing the overflow onto the embankment, and the changes in configuration of the embankment profiles are successively calculated in accordance with the erosion rate of the embankment material as a function of the bed shear stress on the embankment surface.The results of three dimensional analysis of embankment erosion due to overflow are presented in this paper.

2 GOVERNING EQUATIONS

The following shallow water equations are used to describe the behaviour of overflowing water onto an embankment:

$$\frac{\partial \boldsymbol{U}}{\partial t}+\frac{\partial \boldsymbol{F}}{\partial x}+\frac{\partial \boldsymbol{G}}{\partial y}=\boldsymbol{S} \tag{1}$$

in which

$$\boldsymbol{U}=\begin{pmatrix} h \\ uh \\ vh \end{pmatrix},\ \boldsymbol{F}=\begin{pmatrix} uh \\ u^2h+gh^2/2 \\ uvh \end{pmatrix},\ \boldsymbol{G}=\begin{pmatrix} vh \\ uvh \\ v^2h+gh^2/2 \end{pmatrix},$$

$$\boldsymbol{S}=\boldsymbol{S}_0+\boldsymbol{S}_f=\begin{pmatrix} 0 \\ -gh\partial z/\partial x \\ -gh\partial z/\partial y \end{pmatrix}+\begin{pmatrix} 0 \\ ghS_{fx} \\ ghS_{fy} \end{pmatrix} \tag{2}$$

where $\boldsymbol{U}$ is the state variable vector, $\boldsymbol{F}$ and $\boldsymbol{G}$ are the flux vectors, $\boldsymbol{S}$ is the source term vector, h is the flow depth, u and v are the flow velocities along the x and y directions, respectively, g is the acceleration due to gravity, z is the height of the flow bed, respectively, and S_{fx} and S_{fy} are the energy slopes in the x

and y directions, respectively. Energy slopes S_{fx} and S_{fy} can be estimated by using the Manning formula as follows:

$$S_{fx} = \frac{n^2 u\sqrt{u^2+v^2}}{h^{4/3}} \quad , \quad S_{fy} = \frac{n^2 v\sqrt{u^2+v^2}}{h^{4/3}} \tag{3}$$

where n denotes the Manning's roughness coefficient. The above shallow water equations are obtained by integrating the Navier–Stokes equations over the flow depth with the assumptions of the uniform velocity distribution in the vertical direction and the hydrostatic pressure distribution. Although the overflowing water of an embankment does not maintain the hydrostatic pressure distribution when it undergoes rapid changes in the bed slope on the crest, equation (1) is adopted as the governing equation for the water flow onto the embankments for simplicity.

The progression of soil erosion, induced by overland flows, can be described as follows:

$$\frac{\partial z}{\partial t} = -\frac{E}{1-\lambda} \tag{4}$$

where E and λ denote the erosion rate and the porosity of the soil bed, which means the embankment surface here, respectively. The erosion rates of soils are related to the bed shear stress, and previous studies on this topic have found the following relationship between the erosion rates and the bed shear stress:

$$E = \begin{cases} \alpha(\tau - \tau_c)^{\gamma} & \tau \geq \tau_c \\ 0 & \tau \geq \tau_c \end{cases} \tag{5}$$

where α and γ are the material constants for the erodibility of soils and τ_c denotes the critical bed shear stress which determines the onset of bed erosion. Bed shear stress τ is obtained from energy slopes S_{fx} and S_{fy} as follows:

$$\tau = \rho \left| \boldsymbol{S}_f \right| = \rho g h \sqrt{S_{fx}^2 + S_{fy}^2} \tag{6}$$

where ρ is the density of water. In this analysis, the governing equations are the system of the partial differential equations of equations (1) and (4), and the four variables to be solved are h, u, v and z.

3 NUMERICAL METHOD

3.1 *Finite volume method*

So far, several numerical methods have been proposed to solve the shallow water equations. We employ the basic procedure proposed by Yoon & Kang (2004) and apply the concept of the surface gradient method (SGM) by Zhou et al. (2001) to the reconstruction of the state variables. A finite volume approach to unstructured grids is applied to equation (1) and the triangular cells are used for the spatial discretization. As shown in Figure 1, state variables u, v and h are stored at their centroids, while variable z is computed at the vertices of the triangular cells. Integrating equation (1) over the area of the ith triangular cell, the following spatially discretized equations are derived with the aid of the divergence theorem:

$$\frac{d\boldsymbol{U}_i}{dt} = -\frac{1}{A_i}\sum_{j=1}^{3} \boldsymbol{E}_{ij}^{*} \Delta\Gamma_{ij} + \boldsymbol{S}_i \tag{7}$$

where $\boldsymbol{U}_i$, $\boldsymbol{S}_i$ and A_i denote the state vector, the source term vector and the area of the ith cell, respectively, $\boldsymbol{E}^{*}_{ij}$ is the normal flux through the jth side of the cell, and $\Delta\Gamma_{ij}$ is the length of the side. Normal flux $\boldsymbol{E}^{*}_{ij}$ is computed at the cell face by a Riemann

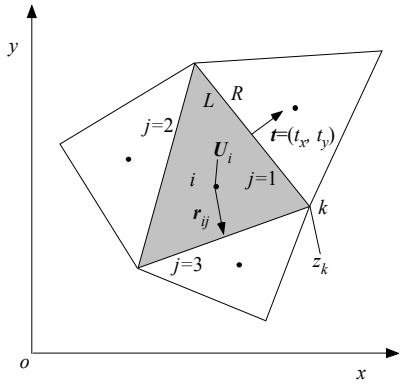

Figure 1. Triangular cells and placement of variables.

solver. This study employs the approximate HLL Riemann solver proposed by Harten et al. (1983), which determines the normal intercell flux as follows:

$$\boldsymbol{E}^{*} = \begin{cases} \boldsymbol{E}_L & 0 \leq S_L \\ \dfrac{S_R \boldsymbol{E}_L - S_L \boldsymbol{E}_R + S_L S_R (\boldsymbol{U}_R - \boldsymbol{U}_L)}{S_R - S_L} & S_L < 0 < S_R \\ \boldsymbol{E}_R & S_R \geq 0 \end{cases} \tag{8}$$

where subscripts L and R mean the left and the right sides of the cell boundary. (The direction of the outward normal vector is considered rightward.) The values with subscripts are defined at the middle of the cell sides and are calculated by the linearly reconstructed data explained later. S_L and S_R are the wave speeds. The detailed procedures for computing the wave speeds and the normal flux are referred to in Yoon & Kang (2004).

3.2 *Linear reconstruction and surface gradient method*

To achieve second-order-accuracy of the numerical computation, the variables, such as u and v, need to be linearly distributed within the finite volume cells, each of which stores their values at the centroids. This procedure is carried out based on the data of the neighbouring cells and is called linear reconstruction. When a variable ϕ is linearly reconstructed on the ith cell, the following procedures are to be completed:

1. The unlimited gradient $\nabla\phi$ of the cell, which means the regular or the ordinary gradient, is evaluated using the data at the centroids of the neighbouring cells.
2. The limited gradient $(\nabla\phi)_i^l$ of the cell is calculated from the unlimited gradients of the cells shearing the interfaces.
3. The following linear interpolation with the obtained limited gradient reconstructs the variable on the cell:
$$\phi_i^{rec}(\boldsymbol{r}_i) = \phi_i + \boldsymbol{r}_i \cdot (\nabla\phi)_i^l \tag{9}$$
where $\boldsymbol{r}_i$ is the position vector relative to the centroid of the ith cell and $\phi_i^{rec}(\boldsymbol{r}_i)$ is the reconstructed variable on the cell as a function of $\boldsymbol{r}_i$.

Details of the above first and second procedures, for calculating the unlimited and the limited gradients, are referred to in Yoon & Kang (2004).

The state variables of the shallow water equation, u, v and h, must be evaluated at the cell interface in order to compute the normal flux given by equation (8). Let the height of water surface η (=h+z) at the ith cell centre be defined as

$$\eta_i = h_i + \frac{1}{3}\sum_k z_k \tag{10}$$

where subscript k is the index for the cell vertices. (Note that the values of z are not stored at the centroids, but at the vertices.) The surface gradient method (Zhou et al. 2001), which guarantees stable computation of steady solutions, gives the state variables at the midpoint of the jth side, $(uh)_{ij}$, $(vh)_{ij}$ and h_{ij}, as follows:

$$(uh)_{ij} = (uh)_i + \boldsymbol{r}_{ij} \cdot (\nabla uh)_i^l \tag{11}$$

$$(vh)_{ij} = (vh)_i + \boldsymbol{r}_{ij} \cdot (\nabla vh)_i^l \tag{12}$$

$$h_{ij} = \eta_{ij} - z_{ij} = \eta_i + \boldsymbol{r}_{ij} \cdot (\nabla \eta)_i^l - z_{ij} \tag{13}$$

where z_{ij} is the height of the flow bed at the midpoint of the jth side of the ith cell, which is obtained as the average of the bed height at the two vertices making the side, and $\boldsymbol{r}_{ij}$ is the position vector from the cell centre to the midpoint of the side. As seen in equations (11) to (13), momentums $(uh)_{ij}$ and $(vh)_{ij}$ on the cell face are directly evaluated with their unlimited gradients, while flow depth h_{ij} is calculated by subtracting z_{ij} from η_{ij} after the height of water surface η_{ij} is evaluated on the cell face with its unlimited gradient.

3.3 Treatment of source term

The source terms in equation (1) are divided into the slope and the friction terms seen as $\boldsymbol{S}_0$ and $\boldsymbol{S}_f$ in equation (2). The treatment of these terms has a great influence on the accuracy of the numerical scheme. When the surface gradient method is employed, adequate attention needs to be paid to balance the first numerical flux term and the second source term on the right-hand side of equation (7) under a steady state. For this purpose, the second and third components of slope term $\boldsymbol{S}_0$ are rewritten in the following form:

$$-gh\nabla z = -g(\eta - z)\nabla z = -g\eta\nabla z + \frac{g}{2}\nabla z^2 \tag{14}$$

Then, these components of the ith cell are numerically evaluated as

$$\left(-gh\nabla z\right)_i = -g\eta_i \left(\nabla z\right)_i + \frac{g}{2}\left(\nabla z^2\right)_i \tag{15}$$

in which

$$\left(\nabla z\right)_i = \frac{1}{A_i}\sum_{j=1}^{3} z_{ij}\Delta\Gamma_{ij}\boldsymbol{t}_{ij} \quad , \quad \left(\nabla z^2\right)_i = \frac{1}{A_i}\sum_{j=1}^{3} z_{ij}^2\Delta\Gamma_{ij}\boldsymbol{t}_{ij} \tag{16}$$

where $\boldsymbol{t}_{ij}$ denote the normal unit outward vector at the jth side of the ith cell. The slope term of $\boldsymbol{S}_0$, calculated from equations (15) and (16), can be balanced with the numerical flux term, and the right-hand side of equation (7) vanishes under the steady condition of no-flow velocity and a constant water level.

In treating the friction source terms, a simple explicit method may induce numerical instabilities when the water depth is very small. To overcome this problem, the friction terms are treated in a fully implicit way with the operator-splitting technique proposed by Yoon & Kang (2004).

$$\frac{d\boldsymbol{U}_i}{dt} = \boldsymbol{S}_{f,i} \tag{17}$$

$$\frac{d\boldsymbol{U}_i}{dt} = -\frac{1}{A_i}\sum_{j=1}^{3}\boldsymbol{E}_{ij}^{*}\Delta\Gamma_{ij} + \boldsymbol{S}_{0,i} \tag{18}$$

The right-hand side of equation (17) includes only friction source terms. Equations (17) and (18) are solved in implicit and explicit ways, respectively.

3.4 Alteration of flow bed elevation

The values of u, v and h are stored at the centroids of the cells, while the values of z are placed at the vertices. The height of flow bed z changes in accordance with the erosion rate of the bed material, which is a function of the bed shear stress related to the flow velocity and the flow depth. Therefore, the values of u, v and h at the vertices must be known and the linearity-preserving interpolation method proposed by Holmes & Connel (1989) is used to calculate their vertex values. From these values at the vertices, the temporal changes in the flow bed are computed by the following equation:

$$\frac{dz_k}{dt} = -\frac{E_k}{1-\lambda_k} \tag{19}$$

which is the ordinary differential equation with respect to t at the kth vertex based on equation (4). The TVD Runge-Kutta scheme was applied for the time integration of the spatially discretized equations (18) and (19), which simultaneously solved the shallow water equations and the temporal changes in the bed height.

4 NUMERICAL SIMULATION

While the governing equations of equations (1) and (4) are solved over the two-dimensional computational domain, i.e., x-y plane, the elevation changes of water surfaces and erosion beds can be succesively computed, which implies that the numerical methods can produce quasi-three-dimensional results over two-dimensional computational domain. This is a great advantage for reducing computational load of three-dimensional numerical analyses which usually need enormous computational effort and time. An example of three-dimensional numerical simulation of embankment breaching induced by the concentration of overtopping water flow is presented herein.

Figure 2 shows the initial profiles of embankment and water surface and the imposed boundary conditions. The embankment has the dimensions of 30cm in height, 130cm in bottom length and 60cm in thickness. The centre of the crest is 2cm lower than the other part to induce the concentration of the overflow. 2,050 finite volume cells with 1096 nodes were used for the spatial discretization. As the boundary conditions for the water flow, the inflow per unit width at a rate of 0.029 $m^3/s/m$ was given from the extreme upstream (the right extreme in Figure 4), and the free outfall condition and the free slip condition were imposed onto the downstream end and the sides of the calculation domain, respectively. The steady flow velocity and flow depth under these boundary conditions were adopted as the initial conditions for the water flow on the embankment. The flow velocity vector field is shown in the x-y plane of Figure 4. For the embankment material properties, a porosity of 0.395, a critical shear stress of τ_c=0.1Pa and erodibility constants of α =8.42×10^{-5} $m/s/Pa^{3/2}$ and γ =1.5 were given. The value of the Manning's roughness coefficient was assumed to be 0.0158.

Figure 3 shows the computed embankment profiles and water surfaces 100 and 600 seconds after the initiation of the embank-ment erosion. As seen in the figure, the central part was dominantly eroded, the overflowing water concentrated there and a flow channel passing through the embankment appeared. The grey cells on x-y plane indicate the dry surface which appeared because of the flow concentration. The numerical results shown in Figure 3 reflect the stability and the feasibility of the proposed method for three-dimensional analysis.

5 CONCLUSIONS

This paper has presented the numerical simulation of embankment erosion caused by overflow. As the governing equations, the two-dimensional shallow water equations were adopted as the governing equations for describing the water flow onto embankments, and the temporal changes in the flow bed were formulated by the erosion rates. The finite volume method was employed for the spatial discretization of the flow domain, and the HLL Riemann solver was used to evaluate the flux through the cell interfaces. The surface gradient method (SGM) was incorporated into the finite volume approach; this enabled the stable computation of the flow field on the erosion surface having complex undulation. The three-dimensional analysis has shown the natural and stable results of embankment breaching which includes the concentration of water flow and embankment erosion, and the creation of the breach channel.

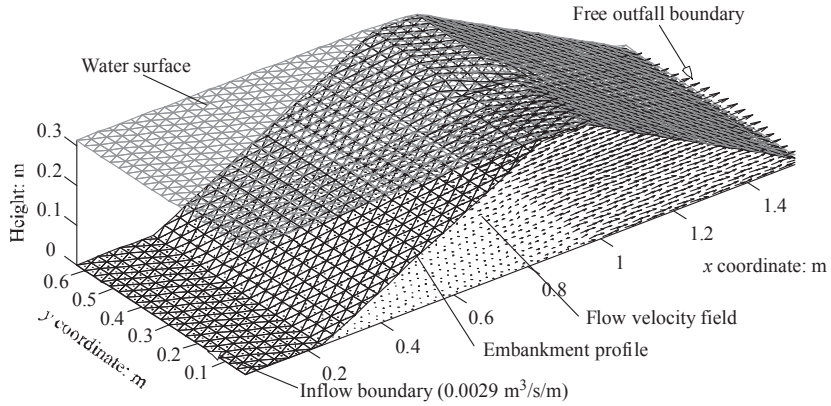

Figure 2. Initial and boundary conditions for three-dimensional simulation.

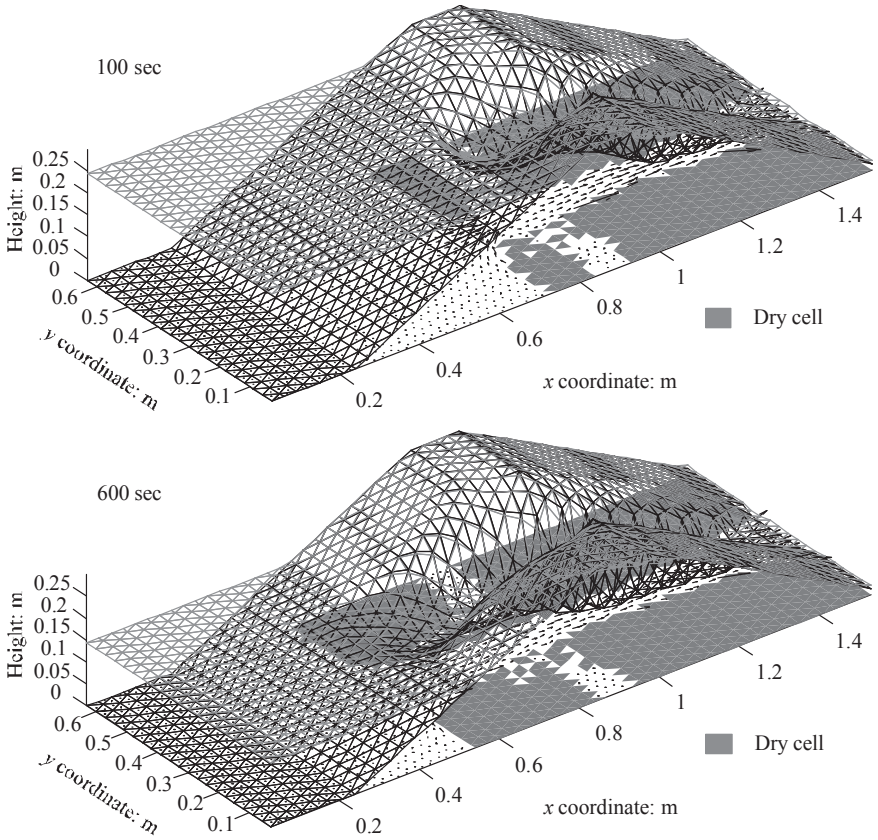

Figure 3. Computed embankment profiles eroded by concentrated water flow (100 and 600 seconds after overflow).

6 REFERENCES

Coleman E. S., Andrews D. P. and Webby M. G. 2002. Overtopping breaching of noncohesive homogeneous embankments. Journal of *Hydraulic Engineering* 128 (9), 829-838.

Foster M., Fell R. and Spannagle M. 2000. The statistics of embankment dam failures and accidents. *Can. Geotech. J.* 37, 1000-1024.

Hanson G. J., Cook K. R. and Hunt S. L. 2005. Physical modeling of overtopping erosion and breach formation of cohesive embankments. *Transactions of the ASAE* 48 (5), 1783-1794.

Hanson G. J., Temple D. M., Hunt S. L., and Tejral R. D. 2011. Development and characterization of soil material parameters for embankment breach. *Applied Engineering in Agriculture* 27 (4), 587-595.

Harten A., Lax P. D., and van Leer B. 1983. On upstream differencing and Godunov-type schemes for hyperbolic conservation laws. *SIAM Rev.* 25 (1), 35–61.

Holmes D. G. and Connel S. D. 1989. Solution of the 2D Navier-Stokes equations on unstructured adaptive grids. *Proc. 9th AIAA Computational Fluid Dynamics Conference*, Technical Papers (A89-41776 18-02), 25-39.

Visser P. J. 1998. *Breach growth in sand dike*. Delft University of Technology, Netherlands, PhD thesis.

Yoon T. H. and Kang S. 2004. Finite volume model for two dimensional shallow water flows on unstructured grids. *Journal of Hydraulic Engineering* 130 (7), 678-688.

Zhou J. G., Causon D. M., Mingham C. G. and Ingram D. M. 2001. The surface gradient method for the treatment of source term in the shallow-water equations. *Journal of Computational Physics* 168,1-25.

Zhu Y. 2006. *Breach growth in clay-dikes*. PhD thesis, Delft University of Technology, Netherlands.